LUND UNIVERSITY
Faculty of Science

Characterization of a Bismuth germanate Anti-Compton Scattering Shield for use with a Germanium COMPEX detector module

Samuel Dawes

Thesis submitted for the degree of Bachelor of Science

Supervised by Daniel Cox (Lund University) and
Dirk Rudolph (Lund University)

Department of Physics
Division of Nuclear Physics
June, 2022

Abstract

The scope of this work is to help determine the functional improvement brought on by introducing a Bismuth germanate (BGO) Anti-Compton Scattering (ACS) shield system to a germanium COMPEX detector module. The COMPEX germanium detector module is already an extremely useful addition in examining gamma-ray spectroscopy. However, by introducing an ACS it is hoped to compound on these improvements yielding an improved sensitivity for full energy peak detection. This was done through different tests using peak-to-compton ratios and peak area-to-total area ratios. The tests including the use of ^{60}Co, ^{137}Cs, and ^{133}Ba sources at various distances with the lead-shielded ACS, the unshielded use of ^{133}Ba at closer distances, probing the germanium crystal with ^{133}Ba across its front face, analysis of ^{133}Ba spectra with a ^{60}Co source to act as background radiation, and the analysis of individual BGO crystals across their length to determine if a more comprehensive characterization of the crystals is required. These tests resulted in a great increase to the full energy peak sensitivity for most distances when lead shielding was in place and comparatively less increase when unshielded. It was also determined that the effect of the ACS was greatest with the source placed in the center of the front face of each individual germanium crystal and that the ACS provides effective protection from background radiation. In addition, detailed characterization of the current BGO crystals is unnecessary as they perform well irrespective of the location of background radiation.

Acknowledgements

I just want to say a massive thank you to the Nuclear Department in general for all their help and support in getting me through the process and the ups and downs. If I was in any other department I am not sure I would have completed this project. A special thank you to Pavel Golubev, Yuliia Hrabar and Luis Sarmiento Pico for the help and making me feel welcome. Further thanks to Dirk and Daniel for going above and beyond as supervisors being supportive both inside and outside of the laboratory.

Contents

1 Introduction

The scintillator invented in 1903 by Sir William Crookes was originally viewed under a microscope to view flashes of light coming from a zinc sulfide screen [1]. Scintillator technology further improved and was useful for being able to visualise the invisible radiation around us. However once the Photomultiplier tube (PMT) was invented in 1944 by Curran and Baker the scintillator began to take on a whole new life [1]. The PMT later allowed for the signal coming from the scintillator to be converted into a digital value which could then be read by a computer leading to a surge in uses for scintillator technology. Once sintillator material began to be manufactured in a reliable way in large enough quantities they began to enter the market as an affordable and accessible method of radiation detection [2].

This leads us to the fact that in recent decades germanium semi-conductor detectors have come to the forefront of gamma-ray spectroscopy. One such system is the recently developed COMPEX germanium detector [3] which is the main component of the new Lundium decay system designed at Lund University. This detector utilises four coaxial cubic composite germanium crystals that form a detector and as effective as it is, these detectors still have the common germanium detector flaw in that there is a high probability that gamma rays will interact with and then escape from the detector before they can be fully absorbed [4]. As they are not fully absorbed into the detector one ends up with a situation where not all counts are shown with the full energy of the event. In gamma-ray spectroscopy this is why peak-to-total ratio is of such great importance. This is a measure of the amount of counts in a peak in a spectrum to that of the background counts. A high peak-to-total ratio means that more of the background radiation is being suppressed and relatively more events are being detected with the correct energy signature [5]. For this reason major importance has been placed upon finding ways to suppress events with incomplete detection.

One method of improving the peak-to-total ratio this is through the use of scintillator technology. One can construct what is known as an Anti-Compton Scattering shield (ACS), which is designed to be placed around a central detector unit. This shield detects photons scattered out of the main detector and interacting with the scintillator crystals. In the setup utilized in this experiment bismuth germanate (BGO) scintillator crystals were arranged around the central germanium detector [6]. These scintillator crystals form the ACS that can record radiation that escapes the main detector, with this one can then compare events occurring in the main detector and in the ACS. Should the event be detected both within the main detector and ACS this event can be removed from both sets of data in a process called 'vetoing'. In this way one can remove entries from the compton background part of the spectrum. This will act as one of the last factors of background suppression of the COMPEX detector along with the inbuilt add-back mechanisms of the COMPEX detector. The add-back mechanism takes interactions that are deposited across several of the germanium crystals and condenses them to a single interaction in one crystal.

With the addition of the ACS and the completion of the Lundium system the further exploration of superheavy elements, the island of stability and the proton drip model can continue with a system that should have significantly better energy resolution and efficiencies at lower photon energies. This is the range where it is predicted that the X-rays emitted during decays of certain superheavy elements (SHE) will be found and so resolution at this scale is important.

The aim of this work is to characterise and better understand the practical workings of the ACS system and probe if there is a need for a more comprehensive study to optimise the design of Lundium. This was done through creating experiments with different tests devised to display the improvement to full energy peak efficiency that the ACS would offer. These tests were then run with the data collected by the Multi Branch System (MBS) software developed by GSI [7] and analysed with the help of the GSI Object Oriented On-line Off-line system (Go4) data analysis software [8].

2 Photon Interactions

For the purpose of this work we are working with high energy photons and thus it is important to understand how they interact with the world around them. There are several different ways in which

photons interact with the world around them. The first is photoelectric absorption, then compton scattering and finally pair production. In the investigations that Lundium will undertake it will examine photons that are either gamma rays or X rays, gamma rays being photons with a energy higher than roughly a few hundred keV and X rays being photons with between a few keV and a few hundred keV. This work will mention gamma rays and X rays frequently. However, it is often used interchangeable with photons.

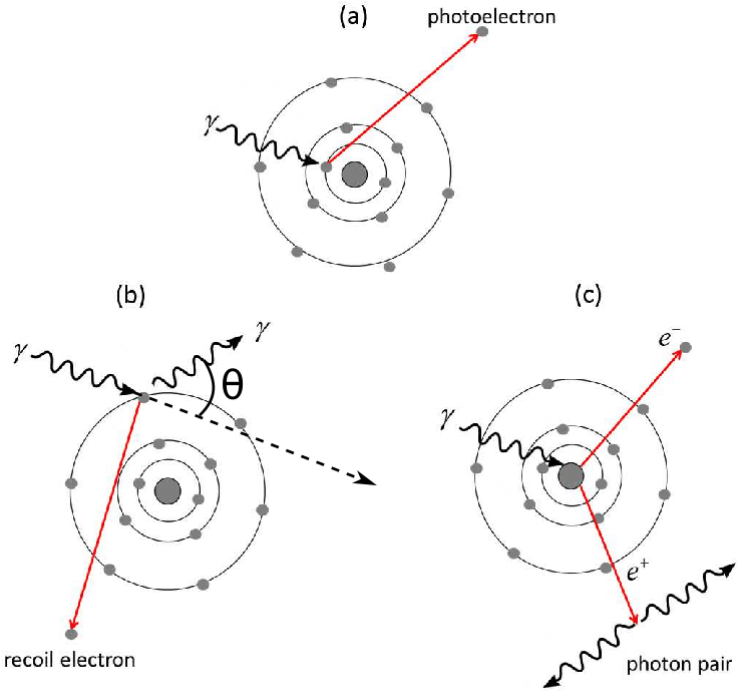

Figure 1: Different modes of gamma-ray interactions [9].

Photoelectric absorption is where a photon will be completely absorbed by the electron of an atom which it interacts with. In this process one has a complete energy transfer between the photon and the electron which leads the electron to have an excited state. This excited electron will then often be emitted from its parent atom as a photoelectron where the energy of the gamma ray is used to overcome the strength of the binding electromagnetic force between the electron and its parent atom and provides significant kinetic energy to the photoelectron. In spectroscopy this is very useful as the energy of the electron E_e can be used to figure out the original energy of the incident photon E_γ due to the fact the the energy of the photoelectron is equal to the energy of the gamma ray minus the binding energy of the electron E_b leading to the equation $E_\gamma = E_e + E_b$ [2]. This is particularly helpful as one can use the energy of the gamma rays to identify the signature decays of different elements.

The next type of interaction is the most common which is the compton effect and also the main focus of this work. When a gamma ray comes into close proximity to an atom they will often interact electromagnetically. This interaction leads to a transfer of momentum and therefore energy from the passing photon and an electron in the outer shell of the atom. We can calculate the energy remaining in the photon after the interaction by using the initial energy of the photon E_γ and the scattering angle, the angle at which the photon is diverted. This leads us to the equation

$$E'_\gamma = \frac{E_\gamma}{1 + \alpha(1 - \cos\theta)} \tag{1}$$

Where alpha is the ratio between the initial energy of the photon and the rest energy of the electron $\alpha = E_\gamma / mc^2$ and θ is the scattering angle of the gamma ray as shown in figure 1 (b). The energy and direction of the gamma ray after scattering is thus determined by the scattering angle and the energy ratio α. After this first event the photon will continue on its path and have potentially many more scattering events until it has dissipated all of its energy.

Using this one can plot out the probability of which direction a gamma ray will scatter based on its original energy. This is shown below in figure 2. Here it is clear to see how dependent scattering angle is on the incident energy of the gamma ray, this is important as as the energy increases the possible scattering angle decreases to the point where backscattering is highly improbable when $\alpha > 4$. For the purpose of this experiment then high energy gamma rays have very little chance to be backscattered out of the detector. The aim of the ACS system is to capture those photons that scatter out of the sides of the main Germanium detector and so it is important that once the gamma rays enter the detector they are either fully absorbed and counted or scatter out through the ACS and are thus discarded.

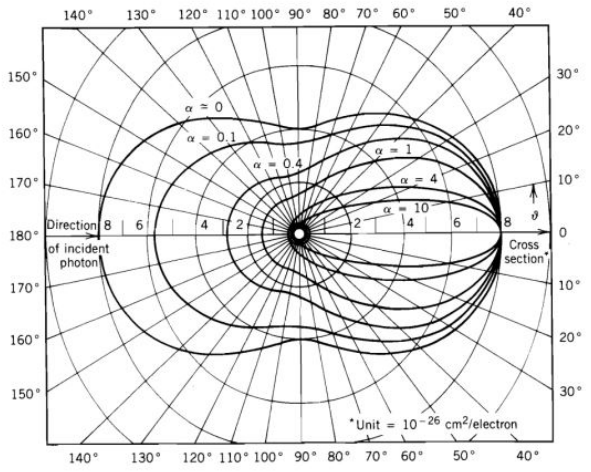

Figure 2: Probability of scattering angles of a gamma ray in a detector [2].

The photon involved in the compton scattering will, in general, transfer much more energy to the electron than the binding energy binding the electron to the atom. This electron will then be ejected from the atom with energy equivalent to the energy transferred minus that of the binding energy of the electron. In the case of the germanium detector this leads to particle-hole pairs which allows for the detection of the scattering event.

The final type of interaction is pair production, this is where a photon can in the presence of matter spontaneously convert its energy into mass to create an electron and a positron of the same mass but opposite charge. These pairs are only generated at high energies and as such will still maintain a high kinetic energy after their creation. In the presence of an electromanetic field that pulls the pair into the real world the two will generally head out in their own directions moving through the detector and losing energy due to interactions with the detector. Once the positron has lost sufficient energy further within the detector it will generally then recombine with an electron through mutual annihilation converting their mass back to energy resulting in two 511 keV photons.

Each of these effects is predominant at different energies, for instance in order of pair production to take place the photon needs to have an energy of at least 1022 keV. Similarly photoelectron absorption will happen closer to lower energies and the compton effect is dominant in most of the mid range areas of energy. This can be seen in figure 3 that shows the relationship between the different interactions at different photon energies and different Z values of the material in which the interactions are taking place.

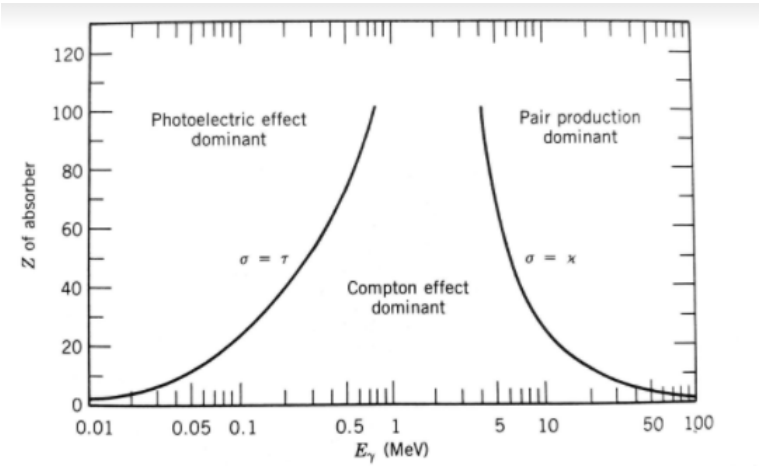

Figure 3: A display of where different gamma interactions are dominant [2].

In this figure we see that the proccess that is dominant is dependent on the energy of the gamma ray and the atomic number of the absorber. The atomic number of the absorber plays a large role as the larger the atom and thus the greater electron density, the greater its cross section of interaction making photoelectric absorption more likely.

These processes are not entirely mutually exclusive and this leads to a variety of situations within our detectors. If were were to take a standard detector and examine what can happen to a gamma ray once it has entered the detector we see which processes lead to a total energy transfer to the detector and which leave a partial energy signature and so adds to background data.

The first situation is where a gamma ray enters the detector and then begins compton-scattering several times within the detector, each time depositing some of its energy. After scattering around in the detector it will then undergo photoelectric absorption. This results in several free electrons which will then deposit all of the gamma ray's initial energy into the detector.

The next situation is where the gamma ray undergoes pair production within the detector splitting into both a positron and an electron. From here they could either recombine and release more photons or they can individually interact depositing their energy in the detector.

3 Semiconductor Detectors

Many of the mainstay detectors in use today for their resolution are semiconductor detectors known for their fine energy resolution. Semiconducting materials will often have four valance electrons which will result crystals bonded with four covalent bonds. With all of the electrons participating in this bonding it means that the valence band is filled. The difference between semiconductor material and insulator material being the small band gap between the valence and conduction band. Due to the low bandgap at room temperature the conduction band is populated as electrons have enough energy to leave their bonds and leave gaps in the bonds.

In order to maximize the conductivity of the semiconducting material one can introduce dopants. These come in the forms of n-type material, material with extra negative charges and p-type materials with extra positive charges. In n-type semiconductors one adds atoms to your semiconducting material with five valence electrons. These will not change the structure of your crystal but will be more willing to donate their spare electron to the conduction band of the semiconductor creating a donor state below the actual conduction band with a smaller gap between it and the valance band. Secondly you can have the case where you have p-type semiconductors, those doped with atoms with three valence electrons. These will create an acceptor state slightly above the valance band where it is easier for electrons to be accepted into the holes again reducing the band gap.

When these two different types of materials comes into contact it creates what is known as a depletion region. This is because the free negative electrons from the n-type semiconductor and the free positive acceptor holes in the material can migrate towards each other and cancel themselves out. This region then has a very small gap between the acceptor states and the donor states making it very

easy for the electrons to get excited. Furthermore if one introduces an negative electric bias across the device one can expand the depletion region as the positive holes migrate to the negative side and the negative electrons migrate to the positive side. While they are trying to migrate they will then cancel each other out creating and even greater depletion region. Therefore once the initial migration has happened one should end up with a stable configuration as shown in figure 4.

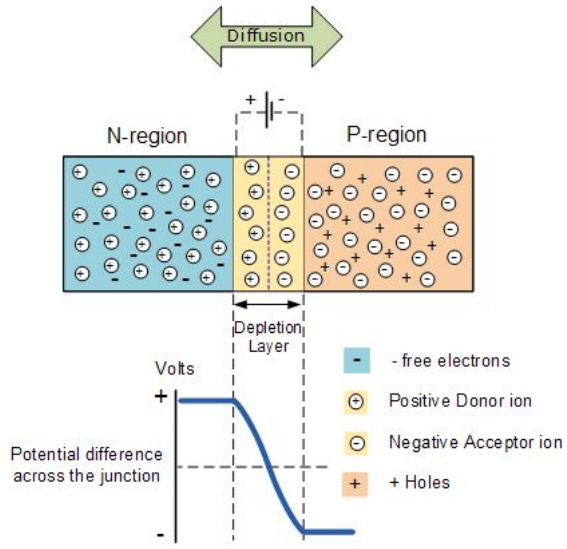

Figure 4: A basic example of the the depletion region of a semiconductor detector [10].

This depletion region is the important part of the detector as this is the area where we want the radiation to strike. When incoming photons interact with the detector it will transfer its energy to an electron which is free to move around within the detector. This electron will then excite many other electrons across the bandgap resulting in a number of particle hole pairs which generate a signal. The number of pairs is approximately equivalent to the energy of the incident photon divided by the energy of the bandgap.

4 Scintillators

Scintillator detectors are another method of detecting radiation. They do this through the process of scintillation, where the striking of a material results in the material fluorescing, releasing a photon around the visible light spectrum. These detectors are comprised of two parts, the scintillator and the PMT. The scintillator can be made of organic or non-organic components and does not have to be a crystal but can also be liquid. The PMT is generally comprised of a photocathode and then dynodes throughout with a anode at the end.

The radiation must first strike the scintillator. In case of gamma-ray radiation the gamma ray must interact with the electrons of the scintilation material with one of the interaction processes described earlier. Similarly to before the incident photon transmits its energy to a electron which then create numerous excitations across the band gap of the scintillator material, which is greater than that of semiconductor material detectors. This process of excitation can be seen in 6. When deexciting from the excited state to the ground state photons are released with the energy corresponding to the band gap. These photons will then bounce around in the scintillator which will then rebound from the insides of the crystal until they hit the photocathode. Once they hit the photocathode they create photoelectrons within the PMT.

Once within the PMT the photoelectrons are attracted to the dynodes along the inside of the PMT. When they hit the dynode they will then excite more photoelectrons before moving to the next dynode and creating even more photoelectrons. This continues down the length of the PMT before the final group of photoelectrons that have been multiplied reach the anode creating an electric pulse.

This pulse will then be proportional to the energy of the original radiation hitting the detector. This process is demonstrated in figure 5

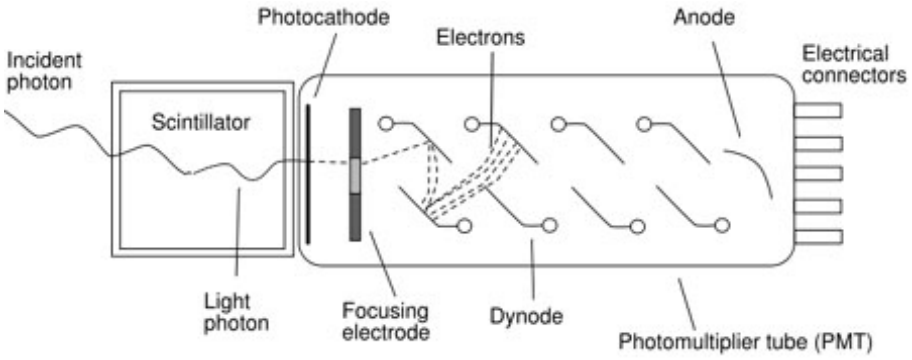

Figure 5: A diagram showing the operation of a scintillator and PMT [11].

Similarly to semiconductor detectors one can take an inorganic crystal and add impurities called activators. These activators create energy states within the bandgap of the crystal which then allow for easier excitation of electrons and emission of photons as the electrons do not need as much energy and also have intermediary steps when it comes to the energy bands as is shown in figure 6.

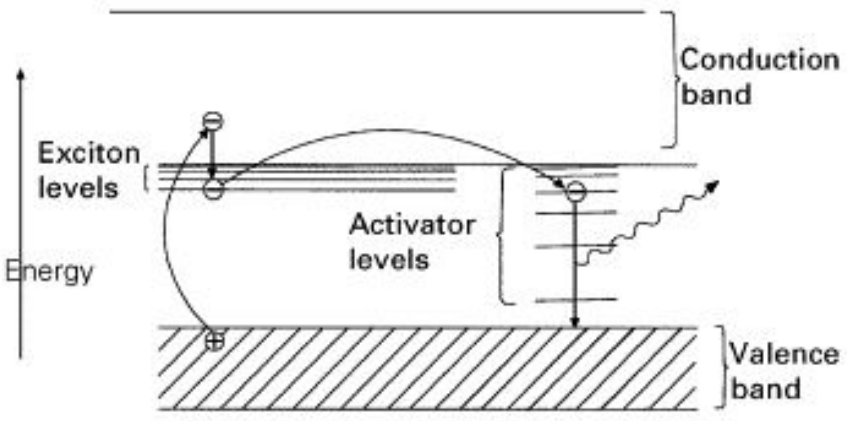

Figure 6: A diagram showing energy levels in a scintillator [12].

5 Analysis of Gamma-Ray Spectra

Figure 7 below is a simple representation of a gamma-ray spectrum that is typical of a detector. This figure is good for displaying the variety of factors that are contained within a gamma-ray spectrum.

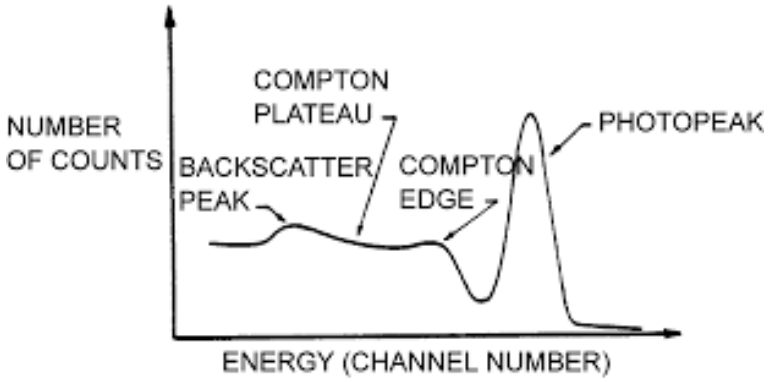

Figure 7: Representation of a gamma-ray spectrum obtained from a detector in this example there is one peak and thus only one gamma-ray energy which creates the entire spectrum [13].

The main feature of a gamma-ray spectrum is the photopeak. In this representation there is only one. However, there could be multiple depending on the signature peaks of the given radioactive decay. In an ideal situation the photopeak would be a single line as all of the incident gamma rays have the exact same energy due to the discrete nature of energy levels. However, upon entering the detector there is statistical spread due to the response of the detector. The more information carriers, e.g., the number of electron-hole pairs in germanium detectors are created the narrower the peak, thus the higher the sensitivity.

The compton plateau is the area of the spectrum which is dominated by counts of scattered gamma rays. As seen before in figure 2, as the gamma ray loses part of its energy there are chances for the scattered gamma ray to leave the detector at any angle. This implies an incomplete energy transfer, and leads to a relatively even distribution of energies at the lower end of the spectra contributing to the area known as the compton plateau. The aim of this project is to see how the addition of the ACS can minimize this area and thus improve the overall sensitivity of the detector especially in low energies where photopeaks can overlap with the compton plateau.

The compton plateau is constrained to the region bound by the compton edge. This edge is defined as the maximum energy that an electron can gain from a scattering event with a gamma ray, where the gamma ray transfers its energy to a electron resulting in a complete backscatter. This energy is given by equation 2 as a direct result of the rearranging of equation 1.

$$E_{max} = \frac{2E_\gamma^2}{mc^2 + 2E_\gamma} \tag{2}$$

The reason for the slight peak at this edge is due to the fact that this is a discrete energy and thus is not able to have energies greater than this resulting in the peak. It is important to note here that while in this situation we have one photopeak and thus the compton edge is clear, when we have multiple photopeaks we end up with a situation where a photopeak can be obscured by a compton edge.

There may also be a secondary bump in the compton plateau that corresponds to the backscatter peak. A gamma ray may interact with something outside the detector and then backscatter resulting in the backscatter peak. The backscatter peak is a result of the compton edge and represents a backscattered gamma ray being reabsorbed by the detector. The backscattered gamma ray will have a discrete energy defined by the maximum energy it had transferred upon its initial scattering event. These gamma rays then may or may not be absorbed by the detector resulting in the full gamma ray being deposited in the detector. The backscatter peak and the compton edge together can contain the full energy of a single gamma ray however one that has been split over two distinct events, hence the two peaks.

The are a few other things that might appear in the gamma-ray spectrum for instance X-rays that occur from decays and from internal conversion. Internal conversion is where a electron is ejected from one of the inner energy bands of an atom and actively competes with gamma-ray emission. After this occurs an electron from an outer electron band will drop down to fill the vacancy, releasing an X-ray

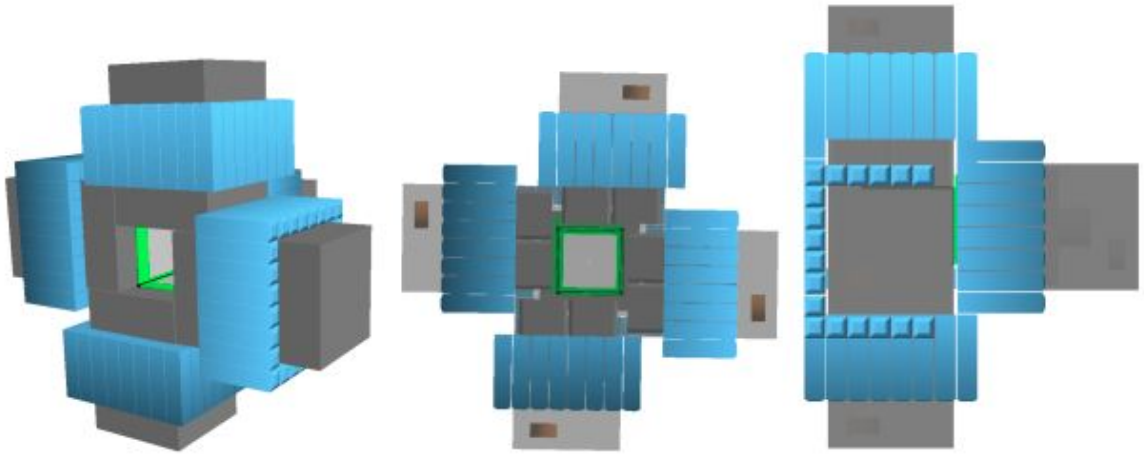

Figure 8: "Renderings of Lundium with ACS including front (middle) and side view (right). 10 BGO bars were removed from the render in the side view to exhibit the front plane of the COMPEX located at the back with its BGOs" [14].

with an energy equivalent to the difference in energy between the vacancy and original orbital of the electron filling the vacancy.

These different features together make up a gamma-ray spectrum and thus it is good to be able to recognise the different extraneous data we are trying to remove through the use of compton suppression and the ACS.

6 Proposed Setup of Lundium

In order to get a larger picture of the detector setup that is being constructed it is useful to view the render in figure 8 which was used as a reference for the construction of Lundium.

Here Lundium is comprised of 5 COMPEX detector modules placed on 5 faces of a cubic vacuum chamber with the sixth face being the opening where the beam of recoil products enters. Each of these faces will be covered with a double-sided silicon-strip detector (DSSSD) which will detect charged particles emitted from decays of implanted recoils while gamma rays will pass through to the COMPEX units. Further it is shown how a potential arrangement of the ACS could be introduced to accommodate the structure of the overall detector. The ACS here functions in most positions as being shielded from direct decay events by either COMPEX units or other BGOs.

7 Experimental Setup

The main experimental approach uses the COMPEX detector along with the BGO ACS. There are 5 measurements that form the basis for this characterization. A study of the different peak-to-compton ratios and peak area-to-totals with lead shielding in place to give the ACS maximum effectiveness, a study of the effectiveness of the ACS for different energy ranges, a study probing different locations on the germanium crystal to see how the ACS performs, a study of how well the ACS will protect COMPEX from background radiation, and a study probing how well the ACS performs with the source at different positions along their lengths.

The COMPEX detector contains the germanium crystals and the pre-amplifier and the electrical cooling for the germanium crystals. The germanium crystals are grouped together and placed into a common vacuum under an aluminium end-cap. These crystals are n-type semiconductor devices implanted with boron which has n+ contacts diffused with lithium located within the boreholes in the backside of the crystals. In order to create the depletion zone a potential of 3500 V is created and to facilitate operation the crystals are cooled to -160 °C [3].

Each crystal has dimensions of 50x50x50 mm^3 arranged in a 2x2 array with 3.9 mm between each other and 5.8 mm behind the aluminum endcap. the borehole is in the centre of the back of each crystal and is 35 mm deep with a diameter of 10 mm as shown in figure 9.

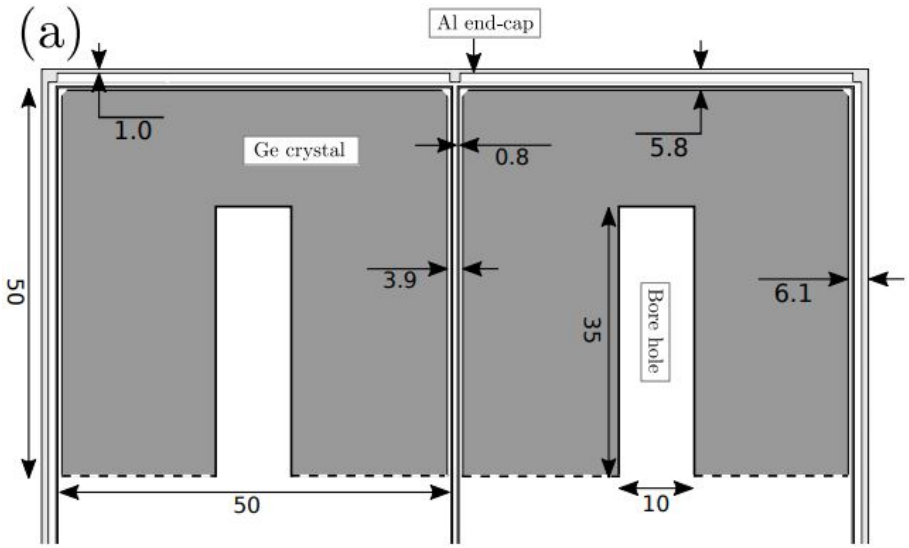

Figure 9: Diagram of Germanium Crystals in the COMPEX detector head [3].

The main component of the ACS will be the Bismuth Germanate crystal sintillators. The ACS is the combination of the wrapped BGO crystals connected to PMTs that are then covered in a 3D-printed shell that holds the detectors surrounding the germanium crystal cap. This is then completely covered by a black sheet wrapping which blocks light and therefore prevents noise in the BGO crystals due to stray photons striking the crystals.

A 3D-printed source holder with a 2 mm deep cylinder bored into the middle of it was used as a way to be able to hold our sources in a uniform manner. This bracket was designed to be the same size as the head of the COMPEX module for easy placement and was then connected to a table stand in such a way as we could then displace the the source relative to the detector in a controlled and reproducible movement. A full picture of the experimental setup can be seen in figure 10.

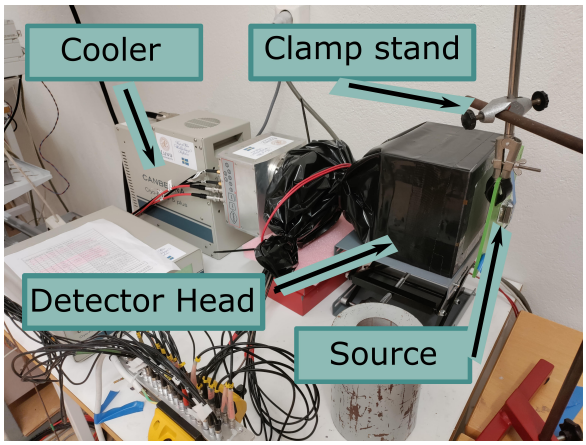

(a) A picture of the full experimental setup.

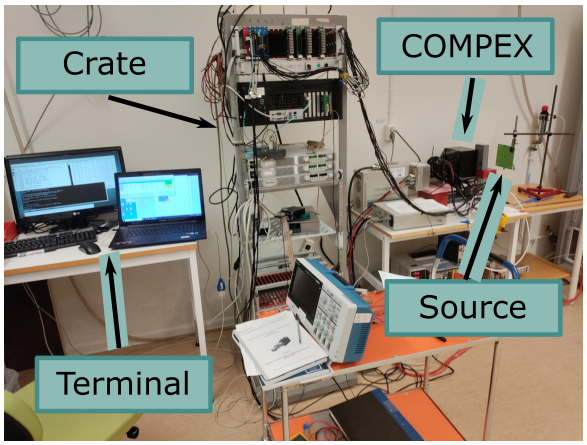

(b) A picture of the COMPEX module and source.

Figure 10: Pictures of the setup.

To begin each experiment the high-voltage power supplies were first turned on and then the detector was given time so that the crystals would reach a new equilibrium temperature. The source was set in order to align with the centre of the four Germanium crystals. However, due to limitations in the number of BGOs currently available the data was acquired from one of the Germanium detectors. As

15 BGO crystals were available, in the setup they were placed surrounding one corner of Germanium crystal that the data was taken from. This setup is suitable for the purposes of testing the experimental setup and making sure that the relative energy efficiency improvement is what is expected. Figure 11 shows the operational components of the detector and ACS, being numbered 0-3 for the germanium crystals and 0-14 for the BGO crystals.

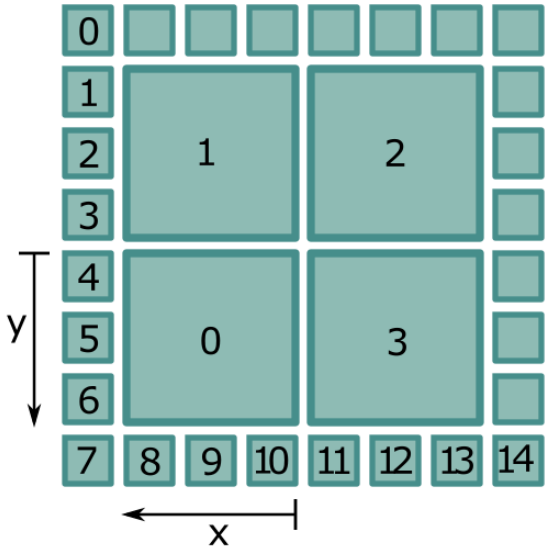

Figure 11: Diagram of the detector elements as seen from the front.

Another required step is that before taking the data and beginning to use it in a productive way the Germanium crystals needed to be calibrated to know the energy response of the detector and identify incoming radiation. In order to do this three sources were utilized to get a wide span of photopeak energies for calibration. The ^{133}Ba source was used for its 81 keV peak, 276 keV peak, 302 keV peak and 356 keV peak as their significant peak amplitude made them easy to discern and assign channels to. Furthermore to get values for a middle energy the 662 keV peak of the ^{137}Cs was used and for high energies the 1173 keV peak and 1332 keV peak were used from the ^{60}Co. The spectra were then analysed using the GSI Object Oriented On-line Off-line system Go4 data analysis software [8]. Using the peak fitting function within Go4 the centroids of these peaks for all four crystals was obtained. After this a calibration curve was created between the channel number and the known energy values of the peaks for each of the crystals as shown in figure 12. This was used to get a set of two linear scaling factors that were used as input values into Go4 for the calibration.

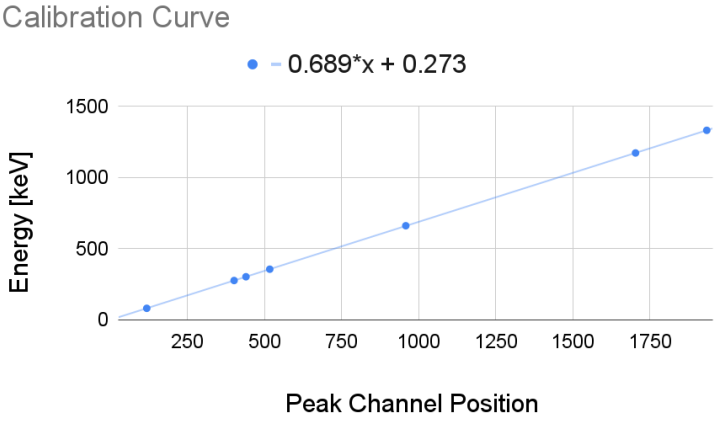

Figure 12: Calibration curve for COMPEX crystal 0 with channel number on the x-axis and energy on the y-axis in keV.

7.1 Efficacy of ACS

In order to perform tests suitable for this experiment the different types of sources had be chosen to represent different energy ranges. For this purpose it was decided to use ^{60}Co for its strong 1332-keV energy peak, ^{137}Cs for its distinctive 662-keV peak and ^{133}Ba for its low energy 81-keV peak [15].

In order to evaluate the efficacy of the Anti-Compton Shield the first step is comparing the peak-to-compton ratio. This ratio is a standard in the industry, it compares the counts found in the maximum bin of the the ^{60}Co 1332keV energy peak to that of the average counts found in the Compton region of the energy spectrum between 1040 keV and 1096 keV as shown in figure 13. To do this Go4 was used to find the total amount of counts in this region which was then divided by the number of channels, in this case 57, to get the compton average. Peak-to-compton ratio was used as this should give a good representation of the efficiency of the Anti-Compton Shield as if operating as expected there should be fewer counts overall in our data but the percentage of those in the peak should be greater.

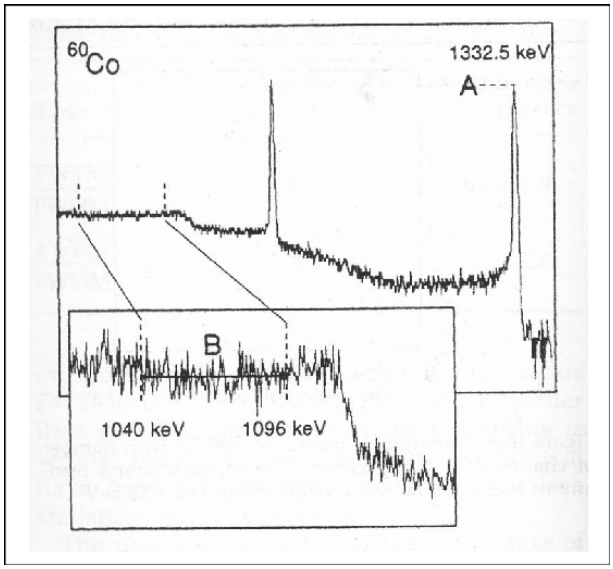

Figure 13: Diagram of the energy spectrum of ^{60}Co where A is the amplitude of the peak and B is the integral over 1040 keV and 1096 keV [16].

In order to calculate the Gaussian fit that would be used in order to find the peak-to-compton ratio the inbuilt Go4 peakfinding system was used between the range of 1300 and 1360 keV such as the example in figure 14. This peak fitting system created a fit of the peak by assuming a Gaussian form for the peaks. From this fitted Gaussian one is given the energy of the peak, which can be used for checking the accuracy of the found peak, the standard deviation which is used to find the FWHM and the amplitude of the peak in counts. To resolve for the FWHM one used the equation

$$\text{FWHM} = 2\sigma\sqrt{2\ln 2}$$

where σ is the standard deviation of the fitted Gaussian. This was then used in order to find the Gaussian integral of the fitted peak with the equation

$$\text{peakint} = a\sigma\sqrt{2\pi}$$

where a is the amplitude of the energy peak.

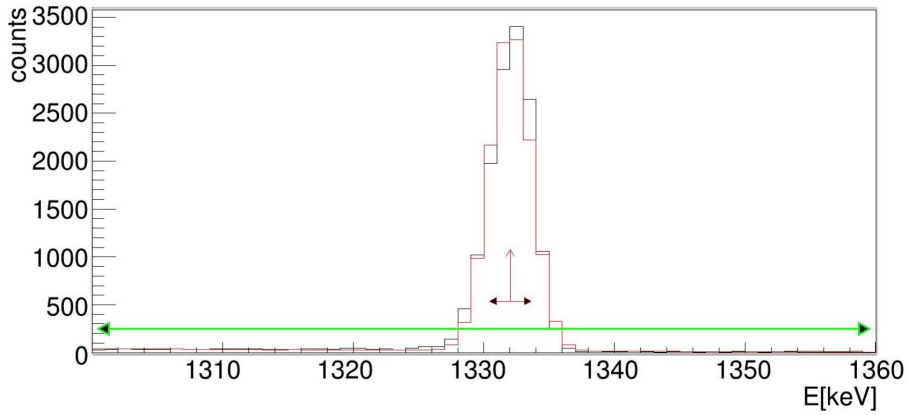

Figure 14: Example of the fitting curve for ^{60}Co between 1300 keV and 1360 keV where the red curve is the Gaussian fit.

For the ^{60}Co source this works well for determining the improvement of the detection at high energy. However, when we look at different sources we required a different metric for determining improvement. For this the peak area-to-total value was chosen as the means to determine improvement. While this has very few equivalences it is useful for showing how the use of the BGO shield can give improvements by a simple comparison between the results when the ACS compton suppression is active versus when the ACS compton suppression is inactive. This will allow an easy means of analysis and allow for a means of assessing how well the ACS is performing. This method is then used for all the other measurements other than ^{60}Co including when the device was purely triggering on the ACS.

To determine the peak area-to-total a standard procedure had to be developed. To this end for each source a range had to be chosen over which to use the peak fitting program. This was done through an iterative process as trying to fit peaks over the entire range results in poor fitting. Furthermore a too restrictive range had the same result while a too large range could see a peak be eclipsed or dominated by a nearby peak. Through this method a standard range was chosen for each source in order to provide useful comparison.

Table 1: Sources and their chosen energy ranges used for standardised peak finder

source	**peak [keV]**	**range used in the peak-finder [keV]**
^{60}Co	1332	1300 - 1360
^{137}Cs	662	640 - 680
^{133}Ba	81	70 - 90

In order then to get a useful value for how well the compton supression was working, it was decided to use a simple method of calculating the percentage improvement between the two values. This was designed in order to present the data in such a way that it is clear to see the improvement between the Compton suppression of the ACS compared to the standard add back of the COMPEX unit.

7.2 Lead Shielding

Using the three different sources at three different positions each, we aimed to compare the effectiveness of the lead shielded BGO's. The aim of having the lead shielding was so that it was extremely difficult for gamma radiation to enter the front face of the BGO's. Any radiation entering from the front would not have been first Compton-scattered through the COMPEX system and so would have its full energy. While not a big problem this would lead to more extraneous data in the ACS and potential for events being suppressed which happened to occur at the same time a stray gamma ray entered the ACS. The sources were suspended from clamps in the bracket so that the sources could be switched out easily without changing the position of the clamp. The lead bricks were placed in front of the

installed BGO crystals at a distance of 2 mm with a 4 mm overlap over the germanium cap. This lead was then placed in such a way as to cover all of the installed BGOs as shown in figure 15. This test is useful for simulating how the detectors will work in practice. As demonstrated in figure 8, all of BGOs should be shielded from direct source exposure by the COMPEX detector modules.

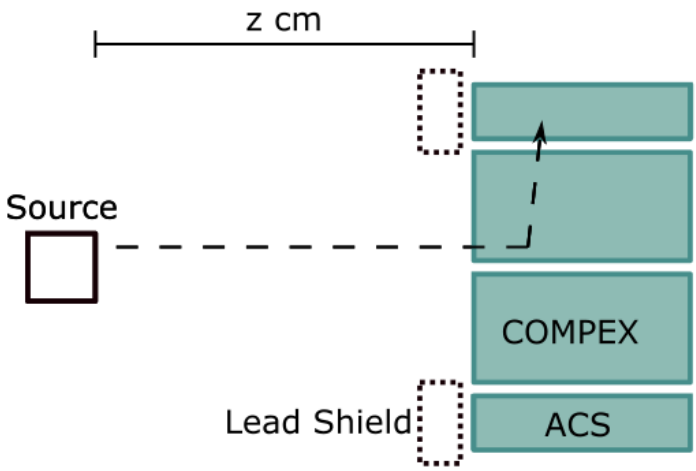

Figure 15: Diagram of the lead shielding setup. This is also the setup for the unshielded experiments just with the lead removed.

This setup was then used to collect data from ^{60}Co at distances of 30 cm 20 cm and 10 cm as well as the industry standard of 25 cm. Then the ^{137}Cs was used with its energy peak at 662 keV at distances of 30 cm, 20 cm, and 10 cm. Then, finally, the ^{133}Ba was used with its energy peak at 81 keV at distances of 30 cm, 20 cm, and 10 cm.

7.3 Unshielded Testing

In this case it was aimed to use the detector in a close replication of how it will be employed in research by removing the lead shielding and then collecting data from ^{133}Ba spectra at distances of 10 cm, 5 cm, 3 cm, and 1 cm. As this was to simulate more standardized conditions these are considered to be the baseline measurements for many of the tests to be performed after this section. The ^{133}Ba spectrum in particular was used for its low energy peak which is especially important for the detection of SHEs who's characteristic decays contain low energy X rays and hence a good full energy peak efficiency is vital. It was especially well monitored at 1 cm as this most closely resembles how the experiments with Lundium will be unshielded. The setup for these measurements is the same as in figure 15 just without the lead shield.

7.4 Germanium Crystal Probing

The aim in this set of tests was to see the variation in the vetoing efficiency if one was to change the placement of the source relative to the germanium face. That is to see the change depending on where the source is on a xy-plane parallel to the face plate. For instance one suggestion was to try and place the source at a position of (26 mm,26 mm), i.e., at the centre of one crystal to measure the vetoing efficiency at this position compared to other positions.

7.5 Background Shielding

This section is designed to test the ability of the ACS to reduce background radiation within the germanium detector itself. This test was how the ACS would protect the germanium crystals while an active detection was taking place. To achieve this a ^{60}Co source was placed perpendicular to the ACS while the ^{133}Ba source was placed at the initial source position as shown in figure 16. Then the distance of the ^{60}Co was varied and finally the position of the ^{133}Ba with regards the the xy-plane parallel to the faceplate was varied.

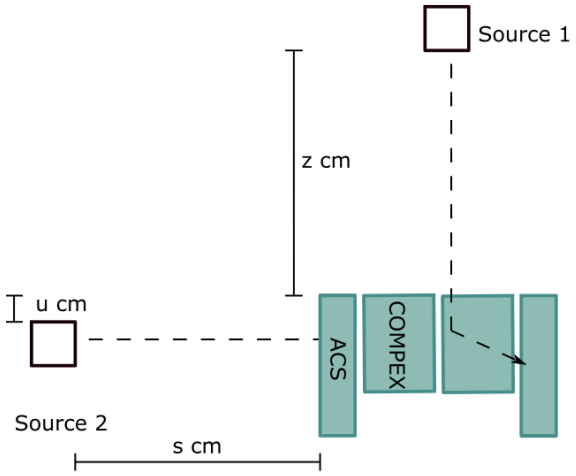

Figure 16: A diagram of the two-source setup.

7.6 ACS Probe

The next part is aimed at trying to assess the need for a further characterization of the ACS and so the measurements were taken directly from the ACS. This utilized the same setup as the previous section just with the ^{133}Ba source removed. The ^{60}Co was kept and its position was varied along the side of the detector. This variable u is shown in figure 16. This was to get a better understanding of how well the ACS functions and whether or not there would be loss of efficiency depending on where the photon comes out of the Germanium and into the ACS. This has the added effect of displaying how different solid angles would affect the recorded spectra.

7.7 Preparation of Analysis

The data from each experiment was compiled into several files within the Aurora computing cluster. From here the files were combined into a single file for each experiment. After this the pre-analysis step was done converting all of the data files into root files which could be quickly executed through the Go4 analysis framework.

8 Analysis

8.1 Lead Shielding

To observe the effect of the compton suppression from the ACS it is useful to visually observe the differences between the spectra. In the spectra below the results from the ^{60}Co while at 25 cm from the detector.

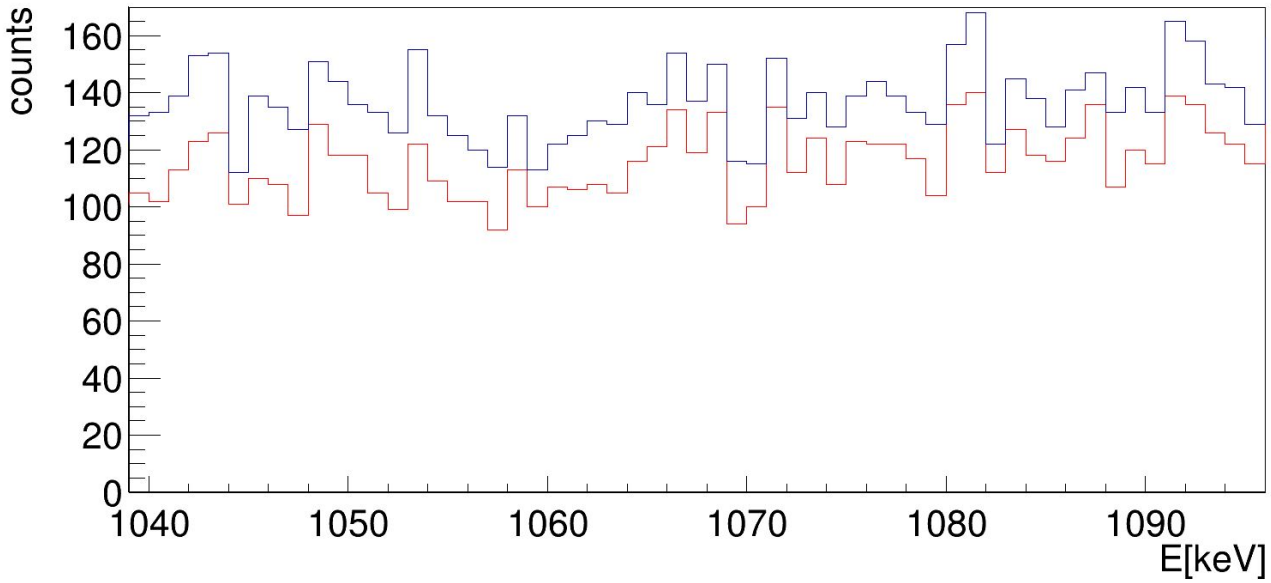

Figure 17: Full ^{60}Co spectrum at 25 cm with compton suppression in red and without compton suppression in blue.

The spectrum shown in figure 17 is zoomed into the area where the compton integral is gained between 1040 and 1096 keV. This is directly related to the peak-to-compton ratio as fewer counts in this area accounts for a greater peak-to-compton ratio. As can be seen there is real difference in the count numbers between suppression and no suppression. In real terms the compton integral without compton suppression is 7653 and with suppression is 6488 which leads to the increase peak-to-compton ratio seen in the tables below. The full spectrum of the ^{60}Co while at 25 cm from the detector is shown in figure 18

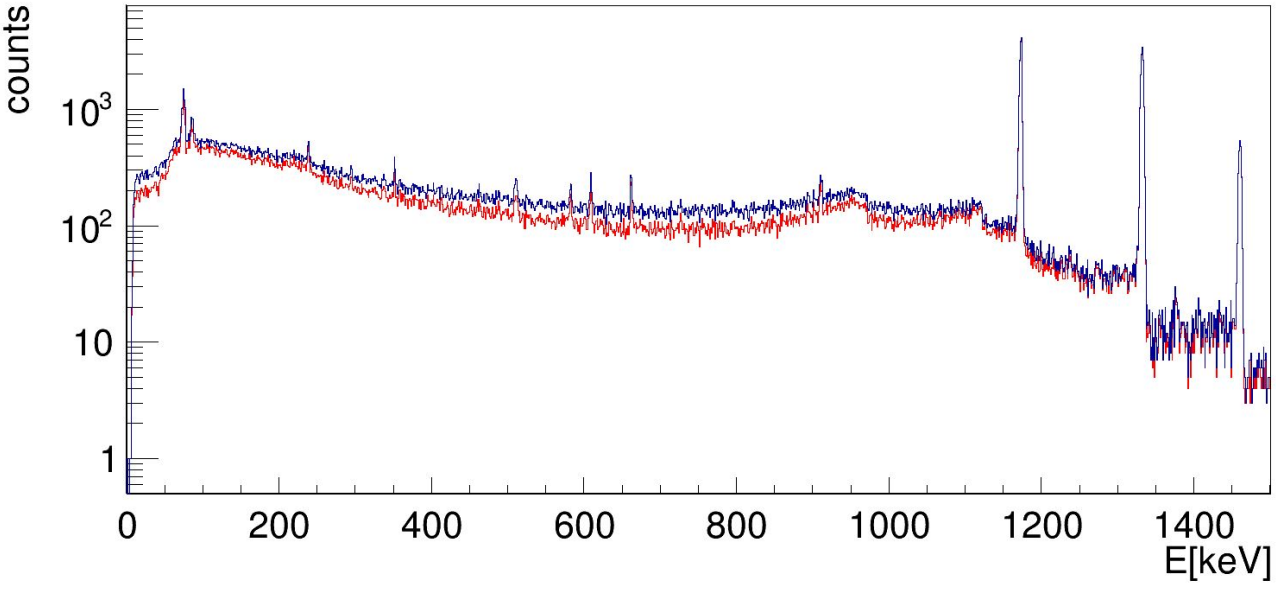

Figure 18: ^{60}Co spectrum at 25 cm with compton suppression in red and without compton suppression in blue.

Table 2: ^{60}Co source measurements with lead shielding, z is the distance between the source and face of the detector as shown in figure 15. The term 'add' refers to addback, and the term 'add anti' refers to addback with vetoing. * This results seems unreasonable possibly as a result of error in the measurement or analysis

z [mm]	**add peak-to-compton ratio**	**add anti peak-to-compton ratio**	**% Improvement**
300	22.99(27)	23.23(24)	1.04(120) *
250	25.35(27)	29.32(32)	13.55(109)
200	26.71(26)	30.66(29)	12.90(98)
100	28.31(22)	31.87(25)	11.14(80)

Here in table 2 it can be ascertained from our data that the ACS provides a vital boost in detection sensitivity which further enhances the performance of the COMPEX detector module. For distances of 25 cm and 20 cm we end up with a percentage improvement of about 13%. However, once we start to get closer around 10 cm there is the potential for there to be a lesser impact as more of the photons enter the centre of the face of the detector expending all their energy in the germanium before they have the chance to enter the ACS. The data point for the 30 cm measurement seems unphysical possibly due to a mistake in the measurement and analysis protocol.

Table 3: ^{137}Cs source measurements with lead shielding, z is the distance between the source and face of the detector as shown in figure 15. The term 'add' refers to addback, and the term 'add anti' refers to addback with vetoing. * This results seems unreasonable possibly as a result of error in the measurement or analysis

z [mm]	**add peak-to-total area ratio**	**add anti peak-to-total area ratio**	**% Improvement**
300	0.2093(38)	0.2441(0044)	14.27(182)
200	0.2194(40)	0.2590(0046)	15.28(178)
100	0.2051(38)	0.2100(0040)	2.29(194) *

Here in table 3 the 662 keV peak of the ^{137}Cs is analysed. This functions as a mid-range energy to assess how well the detectors works at these energies. As can be shown by the results the detector has an very good increase to background suppression at 30 cm and 20 cm. The increase is less pronounced once the distance is closed to 10 cm which seems to be due to the same mistake in measurement and analysis protocol.

Table 4: ^{133}Ba source measurements with lead shielding, z is the distance between the source and face of the detector as shown in figure 15. The term 'add' refers to addback, and the term 'add anti' refers to addback with vetoing.

z [mm]	**add peak-to-total area ratio**	**add anti peak-to-total area ratio**	**% Improvement**
300	0.0587(22)	0.0646(24)	9.15(373)
200	0.0880(31)	0.0998(32)	11.84(320)
100	0.1287(39)	0.1444(35)	10.85(248)

Here in table 4 the ^{133}Ba source is used to analyse how well our setup handles low energy peak efficiency as these are what is important to analyse when looking for the signature decay of SHEs. To begin the source was placed at a maximum of 30 cm. Here it is important to note that our ^{133}Ba source is much less active than that of ^{60}Co. Hence a greater time was taken in the collection of data

and further compounds difficulties due to the low solid angle due to the distance. This means that while we have a lesser increase in the effect of the ACS, it is still present. The improvement gets even better as one gets closer to the detector.

8.2 Unshielded Test

Table 5: ^{133}Ba source measurements without lead shielding, z is the distance between the source and face of the detector as shown in figure 15. The term 'add' refers to addback, and the term 'add anti' refers to addback with vetoing.

z [mm]	**add peak-to-total area ratio**	**add anti peak-to-total area ratio**	**% Improvement**
100	0.1186(33)	0.1229(32)	3.54(266)
50	0.1538(31)	0.1569(38)	2.12(244)
30	0.1554(33)	0.1586(30)	2.03(221)
10	0.1290(27)	0.1345(30)	4.18(223)

Here in table 5 analyses the difference between the ^{133}Ba with the lead shielding present and these new measurements taken without the lead shielding. A visual representation of this difference can be seen in figure 19. At the distance of 10 cm there is a clear difference in the effectiveness when the lead shielding is not present. When the lead is not present the photons are able to enter through the front of the ACS and thus events could be subtracted that happened to hit the detector at the same time as the ACS. In normal operation the source will be closer to the detector module and as such a greater solid angle will go into the detector, with less striking the front face of the ACS reducing these false subtractions. As the improvement continues to increase as the source gets closer it is clear that the ACS is working as intended. During normal operation the front of the ACS should be covered by other components of the Lundium device further reducing false subtractions.

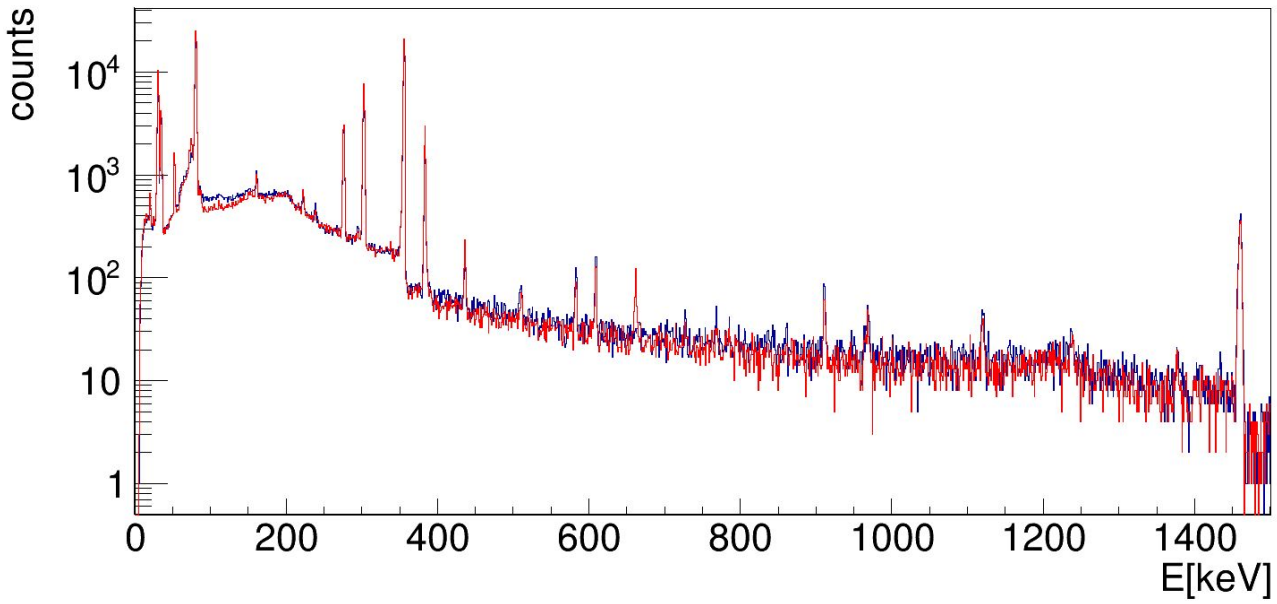

Figure 19: ^{133}Ba spectra with addback and vetoing at 10 cm without lead shielding in blue and with lead shielding in red.

8.3 Germanium Crystal Probing

Table 6: ^{133}Ba source measurements without lead shielding, x,y is the position on the detector face as shown in figure 11. The term 'add' refers to addback and the term 'add anti' refers to addback with vetoing.

x,y [mm],[mm]	**add peak-to-total area ratio**	**add anti peak-to-total area ratio**	**% Improvement**
0,0	0.1290(27)	0.1345(30)	4.18(223)
14,14	0.1645(27)	0.1688(28)	2.56(169)
26,26	0.1764(20)	0.1818(21)	2.96(119)
38,38	0.1765(24)	0.1708(26)	-3.33(155)
14,38	0.1702(19)	0.1771(22)	3.90(128)

Here in table 6 the source was kept at 1 cm but the position in front of the face was varied. Directly in the centre x,y (0,0) the least improvement was expected as here photons from the source have to travel the furthest distance through the germanium making it less likely for the photons to make it to the ACS. Once the source's position is placed over the center of the germanium crystal 0, position (26,26) more of the gamma-rays are entering that crystal than any of the others, this results in the overall peak-to-total area ratio being better and thus a reduced weight to the effectiveness of the ACS. It was also interesting to see that even when the source was positioned directly over the centre of the crystal where the cavity is positioned there was not a pronounced decrease in the effectiveness in the detector. Furthermore when the source was positioned at (38,38) we had a dramatic decrease in the performance of the detector when the ACS was enabled. This is most likely due to the fact there are a lot more gamma-rays directly entering the ACS and therefore a greater chance that the ACS will trigger at the same time as the germanium crystal eliminating otherwise valid events in the germanium. The results for (14,38) however are within the error margins of both the other readings. While this test is important the values for the peak-to-total area ratios are likely to be much higher in the centre (0,0) once data is combined from all other germanium crystals as at the moment (26,26) is functioning as the centre of the detector in use.

8.4 Background Shielding

Table 7: Secondary ^{60}Co source at 90 degrees to detector with a main ^{133}Ba source at different displacements and different x,y placements, where s is the displacement of the side source as shown in figure 16, x,y is the position on the detector face, The term 'add' refers to addback, and the term 'add anti' refers to addback with vetoing.

s [mm]	**x,y [mm],[mm]**	**add peak-to-total area ratio**	**add anti peak-to-total area ratio**	**% Improvement**
100	0,0	0.1141(25)	0.1228(27)	7.09(221)
100	14,14	0.1542(22)	0.16220(25)	4.91(16)
50	0,0	0.0994(23)	0.1122(29)	11.43(259)

Here in table 7 as expected when we introduce a secondary ^{60}Co source our peak to total readings for the detector are not nearly as good as they where when we had no source showing that these events are still making it into the main detector. Below in figure 20 the difference can be seen between the spectra of the ^{133}Ba sample where the side source is not present and where it is present. Even with the ACS present there is still leakage into the detector. Even with this leakage, however, we still get a significant improvement in our peak-to-total values from the presence of the ACS. It is also worth

noting that the peak-to-total values increase as the side source gets further from the ACS meaning that for distant background radiation the ACS should provide adequate protection.

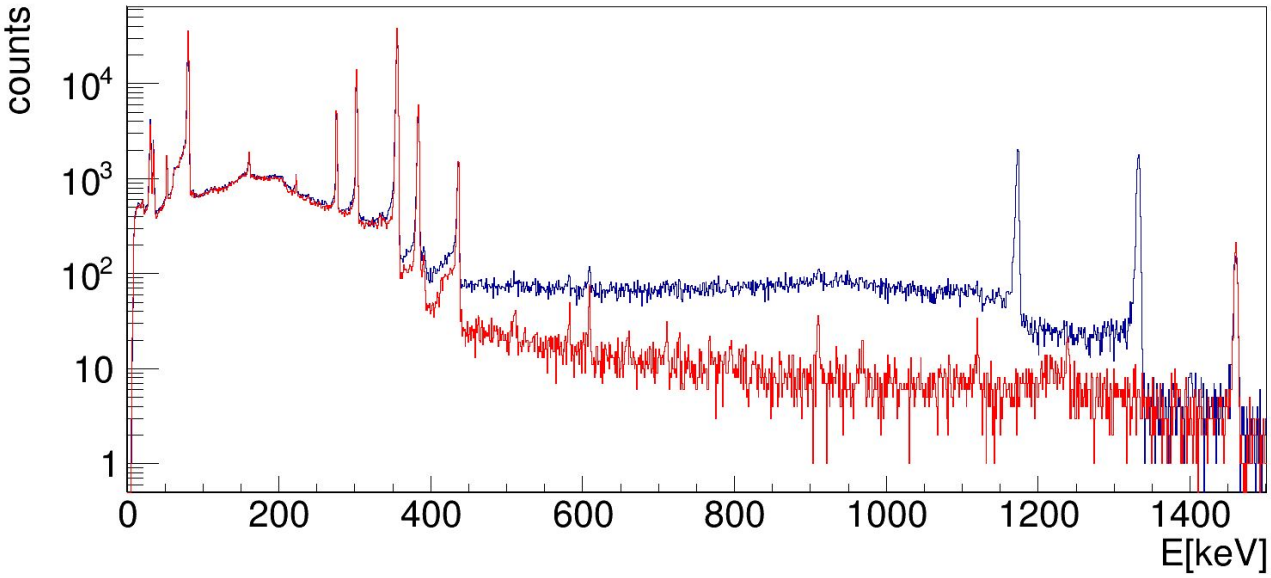

Figure 20: ^{133}Ba spectrum at 1 cm with addback and vetoing without a perpendicular ^{60}Co side source in red and with the perpendicular ^{60}Co side source in blue.

8.5 ACS Probing

From this point it is the ACS that was being triggered in order to determine if a more comprehensive analysis of the ACS is required. Data was taken from all of the triggered BGOs and the following tables are selected so that one can get an overview while the rest can be seen in the appendix. From these the peak-to-totals were taken to see how effective the ACS was at detecting the background radiation. The first selected BGO is BGO crystal 0 shown in figure 11. As the source is located at 0 on the y axis as defined by the figure BGO 0 is at the top and BGO 4 is approximately in the direct path of the gamma-rays from the source. Here we note that the peak-to-totals of these were much more difficult for the program to discern and the energy peak used for the ^{60}Co the 662 keV peak was almost never correctly taken by the fitting program.

Table 8: ^{60}Co source at 90 degrees to detector and energy detection efficiency at different displacements along the side of the BGO 0, where u = 0 is the centre of the shield looking from the side and -u is toward the base of the BGO where it connects to the PMT and +u is toward the front end of the BGO.

u [mm]	**peak energy [keV]**	**peak-to-total area**
-40	667.22(16)	5.14(6)
-20	667.51(18)	5.14(7)
0	667.03(18)	5.18(7)
20	667.98(18)	5.19(7)
40	669.43(17)	5.12(7)

From the results in table 8 it can be seen that when the source is moved along in direction u back and fourth there is little difference in the in the peak-to-total ratio taken from the crystal as the solid angle will vary little from this distance.

Table 9: ^{60}Co source at 90 degrees to detector and energy detection efficiency at different displacements along the side of the BGO 4, where u = 0 is the centre of the shield looking from the side and -u is toward the base of the BGO where it connects to the PMT and +u is toward the front end of the BGO.

u [mm]	**peak energy [keV]**	**peak-to-total area**
-40	672.17(10)	5.16(4)
-20	673.30(11)	5.24(5)
0	673.46(11)	5.26(5)
20	674.42(11)	5.27(5)
40	675.60(10)	5.23(4)

BGO 4 shown in table 9 is where it was expected so see the most variation of the peak-to-total values with u value. This is because as the intensity of the source drops off with distance the closest BGO should see the most variation in intensity when the u value changes, however including error bars the peak-to-total ratio is still relatively consistent with only a minor variation occurring at u -40 where the source is at the end of the BGO crystal near the PMT. Figure 21 visually demonstrates how varying u changes the spectrum displaying visually the small differences.

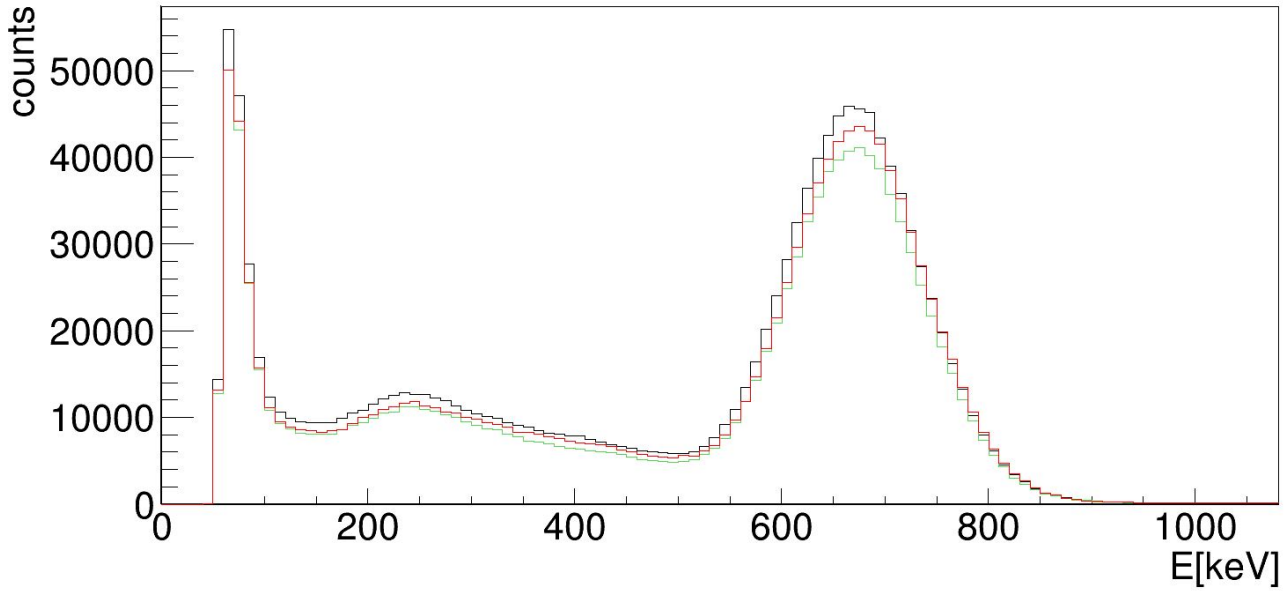

Figure 21: ^{60}Co side source spectrum 5 cm to the ACS at 90 degrees to the detector with u = -40 mm in blue u = 0 mm in green and u = 40 mm in red.

Table 10: ^{60}Co source at 90 degrees to detector and energy detection efficiency at different displacements along the side of the BGO 7, where u = 0 is the centre of the shield looking from the side and -u is toward the base of the BGO where it connects to the PMT and +u is toward the front end of the BGO.

u [mm]	**peak energy [keV]**	**peak-to-total area**
-40	639.24(17)	5.09(8)
-20	640.40(18)	5.13(8)
0	640.15(18)	5.14(8)
20	641.34(18)	5.18(8)
40	642.87(17)	5.12(8)

BGO 7 was selected in order to compare and contrast with BGO 0 as they should have approximately equivalent results for the peak-to-total ratio as they are the same distance from the source however on opposite sides. As is displayed in table 10 compared to table 8 they are similar enough to confirm this and so are functioning as intended.

Table 11: ^{60}Co source at 90 degrees to detector and energy detection efficiency at different displacements along the side of the ACS 8, where u = 0 is the centre of the shield looking from the side and -u is toward the base of the BGO where it connects to the PMT and +u is toward the front end of the BGO.

u [mm]	**peak energy [keV]**	**peak-to-total area**
-40	637.95(64)	2.98(15)
-20	638.55(64)	3.30(16)
0	638.47(65)	3.30(17)
20	639.23(66)	3.34(17)
40	642.61(59)	3.14(15)

BGO 8 is then selected and analysed in table 11 as it sits directly behind BG0 7 and as such is a good display of the amount that gets through BGO 7 and from Germanium crystal 0. Below figure 22 gives a good visual example of the difference between several of the different BGOs depending on their position relative to the source.

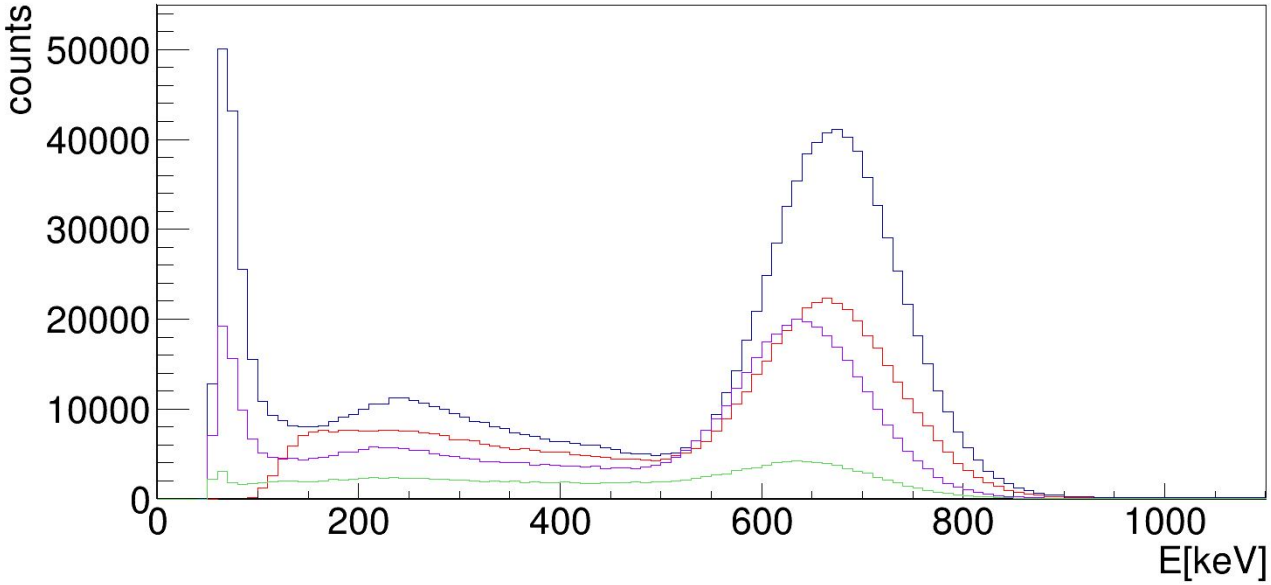

Figure 22: ^{60}Co side source spectrum 5 cm to the ACS at 90 degrees to the detector in BGO 4 in black, BGO 0 in red, BGO 7 in purple and BGO 8 in green, where u = 0 is the centre of the shield looking from the side and -u is toward the base of the BGO where it connects to the PMT and +u is toward the front end of the BGO.

Table 12: ^{60}Co source at 90 degrees to detector and energy detection efficiency at different displacements along the side of the BGO 12 , where u = 0 is the centre of the shield looking from the side and -u is toward the base of the BGO where it connects to the PMT and +u is toward the front end of the BGO.

u [mm]	**peak energy [keV]**	**peak-to-total area**
-40	605.61(515)	2.35(95)
-20	604.82(542)	2.25(100)
0	585.67(992)	3.91(293)
20	591.97(747)	2.66(157)
40	597.99(726)	1.69(104)

BGO 12 was the last BGO to be examined as it was the last BGO which had energy curves that were distinctive enough for the inbuilt go4 fitting program to get results for. As expected the value of the energy peak as shown in 12 was well off the original 662 keV of the source representing the fact that as the gamma-ray travels through the Germanium crystals and other BGO crystals it will interact through compton scattering and lose energy.

9 Conclusion

Through the analysis of the different peak-to-compton and peak-to-total values of each experiment there is a clear improvement through the use of the ACS system. This experiment has also demonstrated that there is no justification for a more extensive analysis into the efficacy of the BGOs as they are efficient enough for the purpose they serve. The ACS is an extremely valuable addition to the COMPEX detector module as it increases the sensitivity while minimizing cost and space usage. While it could be potentially more potent to simply have a greater wall of Germanium detectors in the confines of the Lundium detector setup they are highly effective. The Lundium setup as it stands at the moment will have Germanium COMPEX units on all sides and thus render additional units superfluous. However, the addition of the ACS allows a greater improvement to the sensitivity through its addition. It has long been tradition to introduce ACS modules to detectors to improve them and the ACS discussed in this project is no different. Even though the improvement is reduced at shorter ranges it is still valuable especially at lower energy ranges such as those that are needed in the search for SHEs.

References

[1] Stephen A. Dyer. *Survey of instrumentation and measurement*. J. Wiley, 2001.

[2] Kenneth S. Krane and David Halliday. *Introductory nuclear physics*. Wiley, 1988.

[3] A. Såmark-Roth et al. "Compex: a cubic germanium detector". In: *The European Physical Journal A* 56.5 (May 2020), p. 141. ISSN: 1434-601X. DOI: 10.1140/epja/s10050-020-00155-3. URL: https://doi.org/10.1140/epja/s10050-020-00155-3.

[4] P.J. Nolan, D.W. Gifford, and P.J. Twin. "The performance of a bismuth germanate escape suppressed spectrometer". In: *Nuclear Instruments and Methods in Physics Research Section A: Accelerators, Spectrometers, Detectors and Associated Equipment* 236.1 (1985), pp. 95–99. ISSN: 0168-9002. DOI: https://doi.org/10.1016/0168-9002(85)90131-7. URL: https://www.sciencedirect.com/science/article/pii/0168900285901317.

[5] Tamaki Watanabe et al. "Evaluation of peak-to-total ratio for germanium detectors". In: *Applied Radiation and Isotopes* 50.6 (1999), pp. 1057–1061. ISSN: 0969-8043. DOI: https://doi.org/10.1016/S0969-8043(98)00127-4. URL: https://www.sciencedirect.com/science/article/pii/S0969804398001274.

[6] C.W. Beausang et al. "Measurements on prototype Ge and BGO detectors for the Eurogam array". In: *Nuclear Instruments and Methods in Physics Research Section A: Accelerators, Spectrometers, Detectors and Associated Equipment* 313.1 (1992), pp. 37–49. ISSN: 0168-9002. DOI: https://doi.org/10.1016/0168-9002(92)90084-H. URL: https://www.sciencedirect.com/science/article/pii/016890029290084H.

[7] GSI. "MBS". In: *Welcome to the Multi Branch System (MBS)* (). URL: https://www.gsi.de/en/work/research/experiment_electronics/data_processing/data_acquisition/mbs.

[8] GSI. "Go4". In: *the go4 project page* (). URL: https://www.gsi.de/en/work/research/experiment_electronics/data_processing/data_analysis/the_go4_home_page.

[9] Sun Tao. "Rigid motion correction for head CT imaging". PhD thesis. Feb. 2018.

[10] *PN junction theory for semiconductor diodes*. Jan. 2018. URL: https://www.electronics-tutorials.ws/diode/diode_2.html.

[11] *Research Fundamentals: What are scintillator materials?* 2009. URL: https://web.stanford.edu/group/scintillators/scintillators.html.

[12] A.C. Hannon. "Neutron Diffraction, Instrumentation*". In: *Encyclopedia of Spectroscopy and Spectrometry (Second Edition)*. Ed. by John C. Lindon. Second Edition. Oxford: Academic Press, 1999, pp. 1766–1778. ISBN: 978-0-12-374413-5. DOI: https://doi.org/10.1016/B978-0-12-374413-5.00223-2. URL: https://www.sciencedirect.com/science/article/pii/B9780123744135002232.

[13] *GAMMA-RAY SPECTRA*. URL: https://faraday.physics.utoronto.ca/.

[14] Daesung Cho. *Simulation of Anti-Compton Shield Augmentation to the Lundium Decay Station Using Geant4*. eng. Student Paper. 2019.

[15] *The Lund/LBNL Nuclear Data Search*. Apr. 1998. URL: http://nucleardata.nuclear.lu.se/toi/.

[16] Mei Wo Yii. "Determination performance of Gamma Spectrometry co-axial HPGe detector in Radiochemistry and Environment Group, Nuclear Malaysia". In: Oct. 2014.

10 Appendix

Table 13: Calibration values for each germanium crystal

Germanium crystal	**m**	**b**
0	0.689	0.273
1	0.702	-0.018
2	0.699	0.121
3	0.700	-0.049

Table 14: ^{60}Co source at 90 degrees to detector and energy detection efficiency at different displacements along the side of the BGO 1, where u = 0 is the centre of the shield looking from the side and -u is toward the base of the BGO where it connects to the PMT and +u is toward the front end of the BGO

u [mm]	**peak energy [keV]**	**peak-to-total area**
-40	656.61(12)	5.16(5)
-20	657.38(14)	5.17(6)
0	656.54(14)	5.16(6)
20	658.30(14)	5.19(6)
40	659.40(13)	5.14(6)

Table 15: ^{60}Co source at 90 degrees to detector and energy detection efficiency at different displacements along the side of the BGO 2, where u = 0 is the centre of the shield looking from the side and -u is toward the base of the BGO where it connects to the PMT and +u is toward the front end of the BGO

u [mm]	**peak energy [keV]**	**peak-to-total area**
-40	659.31(13)	5.21(5)
-20	660.84(14)	5.24(6)
0	660.72(14)	5.26(6)
20	661.88(15)	5.27(6)
40	663.15(14)	5.24(6)

Table 16: ^{60}Co source at 90 degrees to detector and energy detection efficiency at different displacements along the side of the BGO 3, where u = 0 is the centre of the shield looking from the side and -u is toward the base of the BGO where it connects to the PMT and +u is toward the front end of the BGO

u [mm]	**peak energy [keV]**	**peak-to-total area**
-40	673.74(14)	5.22(5)
-20	675.05(14)	5.26(6)
0	675.23(14)	5.30(6)
20	676.23(14)	5.28(6)
40	677.33(14)	5.25(5)

Table 17: ^{60}Co source at 90 degrees to detector and energy detection efficiency at different displacements along the side of the BGO 5, where u = 0 is the centre of the shield looking from the side and -u is toward the base of the BGO where it connects to the PMT and +u is toward the front end of the BGO

u [mm]	**peak energy [keV]**	**peak-to-total area**
-40	641.92(19)	5.34(8)
-20	642.68(19)	5.43(8)
0	642.82(19)	5.46(8)
20	643.96(20)	5.49(8)
40	645.25(18)	5.41(7)

Table 18: ^{60}Co source at 90 degrees to detector and energy detection efficiency at different displacements along the side of the BGO 8, where u = 0 is the centre of the shield looking from the side and -u is toward the base of the BGO where it connects to the PMT and +u is toward the front end of the BGO

u [mm]	**peak energy [keV]**	**peak-to-total area**
-40	637.95(64)	2.98(15)
-20	638.55(64)	3.30(16)
0	638.47(65)	3.30(17)
20	639.23(66)	3.34(17)
40	642.61(59)	3.14(15)

Table 19: ^{60}Co source at 90 degrees to detector and energy detection efficiency at different displacements along the side of the BGO 9, where u = 0 is the centre of the shield looking from the side and -u is toward the base of the BGO where it connects to the PMT and +u is toward the front end of the BGO

u [mm]	**peak energy [keV]**	**peak-to-total area**
-40	646.17(82)	2.42(15)
-20	645.26(87)	2.62(18)
0	644.13(89)	2.77(19)
20	644.58(91)	2.72(19)
40	648.10(78)	2.57(16)

Table 20: ^{60}Co source at 90 degrees to detector and energy detection efficiency at different displacements along the side of the BGO 10, where u = 0 is the centre of the shield looking from the side and -u is toward the base of the BGO where it connects to the PMT and +u is toward the front end of the BGO

u [mm]	**peak energy [keV]**	**peak-to-total area**
-40	634.48(182)	1.99(28)
-20	634.61(188)	2.28(33)
0	634.20(215)	2.23(35)
20	636.04(199)	2.02(31)
40	636.05(199)	2.15(33)

Table 21: ^{60}Co source at 90 degrees to detector and energy detection efficiency at different displacements along the side of the BGO 11, where u = 0 is the centre of the shield looking from the side and -u is toward the base of the BGO where it connects to the PMT and +u is toward the front end of the BGO

u [mm]	**peak energy [keV]**	**peak-to-total area**
-40	615.93(406)	1.96(64)
-20	608.85(524)	2.40(103)
0	598.68(706)	3.11(177)
20	610.08(586)	2.16(101)
40	600.63(838)	2.45(162)

Table 22: ^{60}Co source at 90 degrees to detector and energy detection efficiency at different displacements along the side of the BGO 13, where u = 0 is the centre of the shield looking from the side and -u is toward the base of the BGO where it connects to the PMT and +u is toward the front end of the BGO

u [mm]	**peak energy [keV]**	**peak-to-total area**
-40	581.20(629)	2.53(125)
-20	578.38(768)	2.58(160)
0	596.43(615)	1.59(87)
20	535.29(2029)	5.31(645)
40	err	err